ACS OMEGA

http://pubs.acs.org/journal/acsodf

Article

Hybrid Approaches-Based Sliding-Mode Control for pH Process Control

Luis Morales, Juan Sebastian Estrada, Marco Herrera, Andres Rosales, Paulo Leica, Silvana Gamboa, and Oscar Camacho*

Cite This: *ACS Omega* 2022, 7, 45301−45313

Read Online

ACCESS | Metrics & More | Article Recommendations

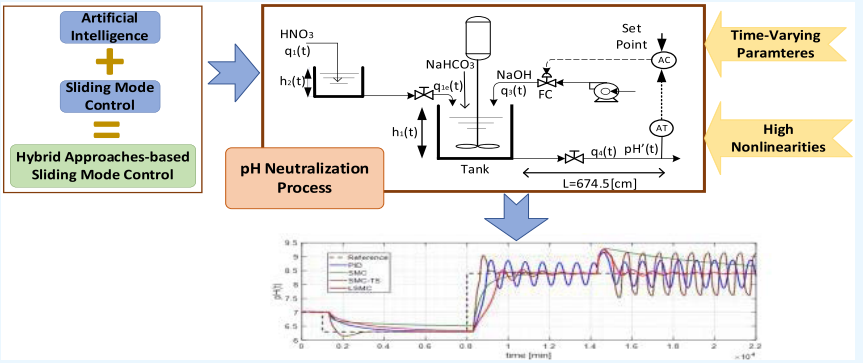

ABSTRACT: This paper presents two hybrid control topologies; the topologies are designed by combining artificial intelligence approaches and sliding-mode control methodology. The first topology mixes the learning algorithm for multivariable data analysis (LAMDA) approach with sliding-mode control. The second offers a Takagi−Sugeno multimodel approach, internal model, and sliding-mode control. The process under study is a nonlinear pH neutralization process with high nonlinearities and time-varying parameters. The pH process is simulated for multiple reference changes, disturbance rejection, and noise in the transmitter. Performance indices are used to compare the proposed approaches quantitatively. The hybrid control topologies enhance the performance and robustness of the pH process under study.

1. INTRODUCTION

pH is the measure of acidity or alkalinity of a solution. Controlling the pH of a process is a regular occurrence in modern industrial applications such as boiler feedwater treatment in thermal power plants, wastewater treatment in the paper and pulp industry, biopharmaceutical manufacturing, and chemical processing. However, controlling pH with a high degree of nonlinearity and time variation is difficult and complex.[1−4] Further, modern process industries require more accurate, robust, and flexible control systems for efficient and reliable operation. There are significant research interests in the pH control problem because of its environmental effects, and also it is a complex problem. The difficulty arises from the high nonlinearity of the process around the neutralization point. The S-shaped titration curve is nonlinearly associated with pH processes.[3] The process gain grows drastically at the intermediate region of the S-shaped curve, i.e., around the neutralization point. This behavior is the primary source of control difficulty.

Moreover, the shape of the titration curve is distorted when the feed condition changes. This situation adds additional complexity to the control system. For this reason, pH control was and even now is challenging work for many researchers.[4]

The control of pH has been studied in the literature; ref 5 addresses the application of an automatically tuned PI algorithm to stabilize the pH value of a pH neutralization process. The proposed adapted PI algorithm uses a simple model to predict the pH closed-loop response and its sensitivity to the PI settings. The information obtained is directly used to adjust the PI tuning parameters online. In ref 6 a fuzzy sliding-mode control (FSMC) is presented as a robust and intelligent nonlinear control technique to control processes with severe nonlinearity and unknown models. The new tuning rule of fuzzy adjusted the proportional and integral constants to adapt to the extreme process condition. Sliding-

Received: September 10, 2022
Accepted: November 17, 2022
Published: December 1, 2022

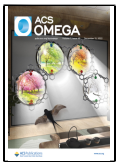

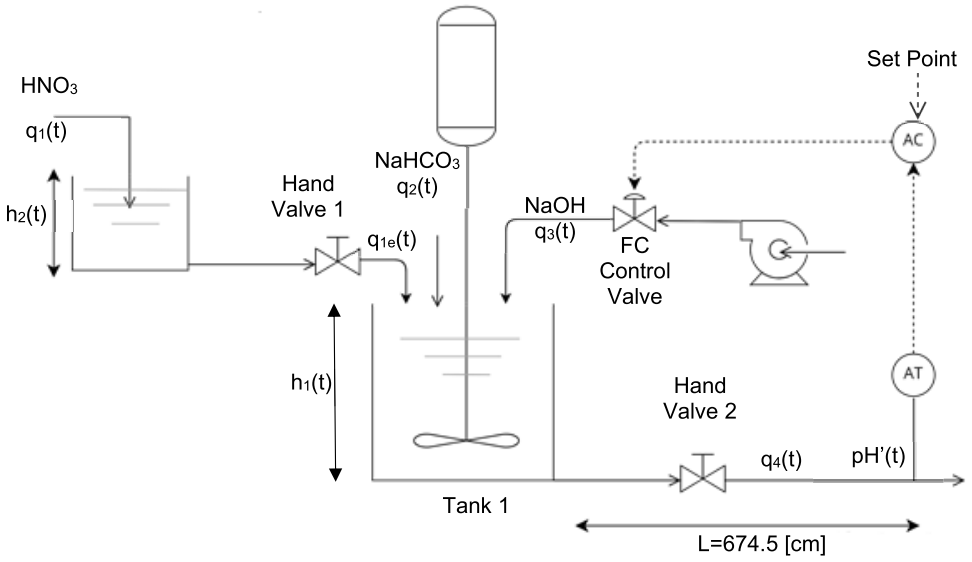

Figure 1. pH reactor with variable delay.

mode control is introduced into classical model-free fuzzy logic control (FLC) for discrete-time nonlinear systems with uncertainty to design a novel fuzzy sliding-mode control to meet the requirement of necessary and sufficient reaching conditions of tuning a pH process. In ref 7 different controllers are designed for the pH neutralization process. The pH system is considered a first-order plus dead time process from the open-loop response. A performance analysis comparison is made among PID, PSO-based I-PD, and MPC. In ref 8 a sliding-mode control (SMC) method is proposed based on loop transfer recovery (LTR) observer for the equivalent first-order model of the pH neutralization process. The nonsingular linear transformations are also used to make delay-free transforms for the time-delay process. At the same time, two observers are designed using LTR. Finally, ref 9 presents an investigation with experimental reports of model predictive control applied to a neutralization pH process.

The advantage of sliding-mode control is that it can overcome the uncertainty of the system and has strong robustness to the disturbance and unmodeled dynamics; especially, it has a good control effect on the nonlinear system. However, the method depends on the state of the system, and there is a control signal chattering phenomenon, especially the chattering phenomenon of the control signal, that seriously affects its practical application. There are two main ways to reduce the chattering phenomenon of sliding-mode control: dynamic sliding-mode control (DSMC)[10−12] and smoothing functions.[13,14] Sliding-mode control (SMC) has advanced to deal with uncertainties and has become well-known within the control community to the point that SMC is being used in several engineering fields. One can find applications in electrical engineering,[15,16] robotics,[17−20] and controlling chemical processes.[21,22] Ref 23 has been used for several chemical processes, for example, refs 24−29.

Since the pH process is highly nonlinear, the idea of the multimodel approach offers a way to build multimodels of the process based on the input−output data or the original mathematical model of the system facing the complexity and nonlinear factors of this system. Therefore, the fuzzy model proposed by Takagi and Sugeno (T-S) expressing the local dynamics of each fuzzy rule by a linear system model can be combined with the robustness of SMC in such a way that the stability of the system can be achieved by a fuzzy combination of the linear system models.[30]

The multimodel control problem has been widely studied in chemical process control. Various studies[31−44] describe control techniques known as multimodel or multilinear control strategies. In the previous references, there are a variety of control techniques, such as adaptive, cascade, sliding mode, and fuzzy. However, to our knowledge, there are no controller combinations as proposed in this work.

A new methodology that combines fuzzy logic with SMC is presented in refs 45 and 46. This technique uses the LAMDA (learning algorithm for multivariable data analysis). LAMDA computes two parameters to identify the states of the system and calculate the control output. First, the marginal adequacy degree (MAD) is obtained as the contribution of the descriptors of an individual to each class with fuzzy probability functions. The MADs of the individuals in each class are combined with fuzzy aggregation operators, resulting in the global adequacy degree (GAD). The GAD is a numerical array with values ranging from 0 to 1; these values quantify the membership degree of the system state (object in LAMDA) to the system classes; thus, LAMDA assigns the object to the most suitable class.

LAMDA has been used to detect functional states of systems,[47,48] which, in general terms, is considered a classification task.[49] In the most recent research, we have proposed LAMDA working as a controller, adding to the algorithm a T-S (Takagi−Sugeno) inference stage to the GADs to obtain a class-based controller.[46] This controller has been tested in processes of nonlinear characteristics, including a considerable dead time. Nevertheless, the proposal has shown promising results in the different tests considering that the plant's mathematical model is not required for the design of the controller.[50,51]

This paper provides two hybrid control topologies developed by merging artificial intelligence techniques with sliding-mode control methods. The first topology combines the LAMDA and sliding-mode control approaches. The second provides a Takagi−Sugeno multimodel strategy, an internal model, and sliding-mode control. The studied process is a

https://doi.org/10.1021/acsomega.2c05756
ACS Omega 2022, 7, 45301−45313

nonlinear pH neutralization process characterized by strong nonlinearities and time-varying parameters. Multiple reference changes, disturbance rejection, and noise in the transmitter are simulated for the pH process. To quantitatively compare the offered methodologies, performance indices are employed. The hybrid control topologies improve the performance and reliability of the investigated pH process. The main contribution of this manuscript can be summarized as follows:

Two new control topologies for pH processes are presented. The first topology mixes the LAMDA approach with the sliding-mode control methodology. The second one offers a combination of Takagi−Sugeno multimodel, internal model, gain scheduling, and sliding-mode control. The resulting hybrid control strategies produce hybrid controllers that improve the performance of this process.

The paper is divided as follows: Section 2 describes the process under study and Section 3 shows fundamental concepts about sliding-mode control and the two artificial intelligence approaches. Then, in Section 4, the design of both proposal approaches is described. Then, in Section 5, results simulation considering performance evaluation are presented, and finally, some conclusions are offered.

2. DESCRIPTION OF THE SYSTEM: PH NEUTRALIZATION REACTOR

The process involves conducting a fluid neutralization reaction with variable liquid volume.[52,53] The process presents dominant delay and time-varying parameters. The change consists in increasing the length of the pipe and, therefore, the distance of the location of the pH transmitter so that, in this way, the time delay $t_0(t)$ also increases.

The operation of the process is as follows: a basic stream flow $q_3(t)$ is manipulated through a valve to be mixed with an acid stream flow $q_1(t)$ and obtain an output flow $q_4(t)$ with a value of pH required; while a constant flow of buffer stream $q_2(t)$ allows keeping the pH value insensitive to small additions of acids or bases. The pH transmitter is calibrated to operate in a range of 2.712−10.75 and is installed 674.5 cm away from the reactor, which generates a time delay in the measurement. Figure 1 indicates the outline of the process, and the following considerations are accepted:

- The volume of the liquid varies without overflowing from the reactor.
- The reactor content is well mixed.
- The reactor and pipeline are well insulated.
- There is complete solubility of the ions of the chemical compounds involved.
- The primary disturbance is the acid stream flow $q_1(t)$.

The following chemical reactions take place inside the pH neutralization reactor

$$H_2CO_3 \leftrightarrow HCO_3^- + H^+ \tag{1}$$

$$HCO_3^- \leftrightarrow CO_3^{2-} + H^+ \tag{2}$$

$$H_2O \leftrightarrow OH^- + H^+ \tag{3}$$

The corresponding equilibrium constants are

$$K_{a1} = \frac{[HCO_3^-][H^+]}{[H_2CO_3]} \tag{4}$$

$$K_{a2} = \frac{[CO_3^{2-}][H^+]}{[HCO_3^-]} \tag{5}$$

$$K_w = [H^+][OH^-] \tag{6}$$

Chemical equilibrium is modeled by introducing two invariant reactions W_a and W_b for each inflow. The reaction W_a is an amount related to the charge of the ions, while W_b indicates the concentration of the ion O_3^{2-}. The invariant reactions are as follows

$$W_{ai} = [H^+]_i - [OH^-]_i - [HCO_3^-]_i - 2[CO_3^{2-}]_i \tag{7}$$

$$W_{bi} = [H_2CO_3]_i + [HCO_3^-]_i + [CO_3^{2-}]_i \tag{8}$$

where i goes from 1 to 4 and represents the flows that act in the process.

Through the equations of equilibrium constants and invariant reactions, an expression to determine the pH level can be found.

$$W_b \frac{\frac{K_{a1}}{[H^+](t)} + \frac{2K_{a1}K_{a2}}{[H^+](t)^2}}{1 + \frac{K_{a1}}{[H^+](t)} + \frac{K_{a1}K_{a2}}{[H^+](t)^2}} + W_a + \frac{K_w}{(t)} - [H^+](t) = 0 \tag{9}$$

$$pH(t) = -\log[H^+](t) \tag{10}$$

The pH is a measure of the hydrogen ions $[H^+]$. The mathematical equations that describe the dynamic behavior of the process are presented.

(a) Mass balance in tank 2.

$$q_1(t)\rho - q_{1e}(t)\rho = A_2\rho\frac{dh_2(t)}{dt} \tag{11}$$

(b) Manual valve.

$$q_{1e}(t) = C_{V2}\sqrt{h_2(t)} \tag{12}$$

(c) Mass balance in the pH neutralization reactor.

$$q_{1e}(t)\rho + q_2(t)\rho + q_3(t)\rho - q_4(t)\rho = A_1\rho\frac{dh_1(t)}{dt} \tag{13}$$

(d) Equation of manual valve 4.

$$q_4(t) = C_{V4}(h_1(t))^n \tag{14}$$

(e) Expression for the invariant reaction W_a based on the application of mass balance in each species of ion.

$$q_{1e}(t)W_{a1} + q_2(t)W_{a2} + q_3(t)W_{a3} - q_4(t)W_{a4}(t) = A_1\frac{d(h_1(t)W_{a4}(t))}{dt} \tag{15}$$

(f) Expression for the invariant reaction W_b based on the application of mass balance in each ion species.

$$q_{1e}(t)W_{b1} + q_2(t)W_{b2} + q_3(t)W_{b3} - q_4(t)W_{b4}(t) = A_1\frac{d(h_1(t)W_{b4}(t))}{dt} \tag{16}$$

https://doi.org/10.1021/acsomega.2c05756
ACS Omega 2022, 7, 45301−45313

Table 1. Design Parameters and Steady-State Values

variable	value	variable	value
$\overline{q_1}$	16.6 mL/s	K_T	7.1429 %
$\overline{q_{1e}}$	16.6 mL/s	K_V	0.3 (mL/s)/%CO
$\overline{q_2}$	0.55 mL/s	A	6.01031 cm^2
$\overline{q_3}$	15.6 mL/s	L	674.5 cm
$\overline{q_4}$	32.75 mL/s	$[q_1]$	0.003 M HNO_3
ref	7.025	$[q_2]$	0.03 M $NaHCO_3$
$\overline{pH}$	7.025	$[q_3]$	0.003 M NaOH + 0.00005 M $NaHCO_3$
ρ	1 mL/cm^3	K_{a1}	4.47×10^{-7}
A_1	207 cm^2	K_{a2}	5.62×10^{-11}
A_2	42 cm^2	K_w	1×10^{-14}
$\overline{h_1}$	25.5 cm	W_{a1}	0.003 M
$\overline{h_2}$	3 cm	W_{b1}	0 M
C_{V2}	9.584 (mL/s)/$cm^{1/2}$	W_{a2}	−0.03 M
C_{V4}	4.5861 (mL/s)/$cm^{0.607}$	W_{b2}	0.03 M
n	0.607	W_{a3}	-3.05×10^{-3} M
c	50.18%	W_{b3}	5×10^{-5} M
$\overline{m}$	52%	W_{a4}	-4.36×10^{-4} M
τ_T	15 s	W_{b4}	-5.276×10^{-4} M
τ_V	6 s		

(g) The time delay between the pH neutralization reactor and the location of the pH sensor.

$$\mathrm{pH}'(t) = \mathrm{pH}(t - t_0(t)) \tag{17}$$

(h) Time delay.

$$t_0(t) = \frac{LA\rho}{q_4(t)} \tag{18}$$

(i) pH transmitter

$$\frac{dc(t)}{dt} = \frac{1}{\tau_T}[K_T \mathrm{pH}'(t) - c(t)] \tag{19}$$

(j) Equation of the control valve.

$$\frac{dq_3(t)}{dt} = \frac{1}{\tau_V}[K_V m(t) - q_3(t)] \tag{20}$$

where:

$q_1(t)$: acid stream flow, mL/s.
$q_{1e}(t)$: outlet acid stream flow from tank 2, mL/s.
$q_2(t)$: buffer stream flow, mL/s.
$q_3(t)$: basic stream flow, mL/s.
$q_4(t)$: output stream flow, mL/s.
$\mathrm{pH}(t)$: hydrogen potential of the liquid in the reactor, dimensionless.
$\mathrm{pH}'(t)$: $\mathrm{pH}(t)$ considering the time delay $t_0(t)$, dimensionless.
$t_0(t)$: time delay, s.
ρ: density, mL/cm^3.
A_1: pH neutralization reactor cross-section, cm^2.
A_2: cross-section of tank 2, cm^2.
$h_1(t)$: liquid level in the pH neutralization reactor, cm.
h_2: liquid level in tank 2, cm.
C_{V2}: flow coefficient of manual valve 2, $(mL/s)/cm^{1/2}$.
C_{V4}: flow coefficient of manual valve 4, $(mL/s)/cm^{0.607}$.
n: manual valve coefficient 4.
$c(t)$: pH transmitter output signal on a scale from 0 to 100%.
$m(t)$: controller output 0 to 100, %.
τ_T: pH sensor time constant, s.
τ_V: control valve time constant, s.
K_T: pH sensor gain, %.
K_V: control valve gain, (mL/s)/% C.O.
A: pipe cross-section, cm^2.
L: pipe length, cm.

3. CONTROLLER FUNDAMENTALS

3.1. LAMDA Sliding-Mode Control (LSMC). The design considers a SISO (single-input, single-output) nonlinear system, represented in state space as

$$\dot{x}_i(t) = x_{i+1}(t), \quad i = 1, \cdots, n-1$$
$$\dot{x}_n(t) = A(X(t), t) + b(X(t), t)u(t) + d(t) \tag{21}$$

where $A(X(t),t)$ and $b(X(t),t)$ are nonlinear functions, $X(t)$ is the state vector of the system, $u(t) \in \mathbb{R}$ is the control input, and $d(t) \in \mathbb{R}$ is the unknown disturbance.

The control action is obtained using the following assumptions:[54] the states of the system $X(t)$ are measurable, $|A(X(t),t)| \le \beta_A$, $b(X(t),t) \neq 0$, and $|d(t)| \le \beta_d$, with β_A and β_d unknown positive constants (Table 1).[55]

The control objective is to bring the system output to the desired state $X_d(t)$ in the presence of model uncertainties and external disturbances.

Considering the desired state $X_d(t)$, the tracking error is defined as

$$E(t) = X_d(t) - X(t) \tag{22}$$

Then, the controller is designed such that for any desired state $X_d(t)$, the tracking error should satisfy

$$\lim_{t\to\infty} \|E(t)\| = \lim_{t\to\infty} \|X_d(t) - X(t)\| \to 0 \tag{23}$$

Based on the fundamentals of the sliding-mode control (SMC), we select a suitable sliding surface[13,22] defined as

https://doi.org/10.1021/acsomega.2c05756
ACS Omega 2022, 7, 45301−45313

Table 2. Rule Table of LSMC for $\dot{s}(t)$

	$\dot{s}(t)$				
	NB	NS	Z	PS	PB
$b(X(t), t) > 0$	γ_1 = NB	γ_2 = NS	γ_3 = ZE	γ_4 = PS	γ_5 = PB

Table 3. Rule Table of LSMC for $s(t)$ and $\dot{s}(t)$ with $b(X(t), t) > 0$

		$\dot{s}(t)$				
		NB	NS	ZE	PS	PB
$s(t)$	PB	γ_5 = ZE	γ_{10} = ZE	γ_{15} = PS	γ_{20}= PB	γ_{25} = PB
	PS	γ_4 = ZE	γ_9 = ZE	γ_{14} = PS	γ_{19} = PB	γ_{24} = PB
	ZE	γ_3 = NB	γ_8 = NS	γ_{13} = ZE	γ_{18} = PS	γ_{23} = PB
	NS	γ_2 = NB	γ_7 = NB	γ_{12} = NS	γ_{17} = ZE	γ_{22} = ZE
	NB	γ_1 = NB	γ_6 = NB	γ_{11} = NS	γ_{16} = ZE	γ_{21} = ZE

$$s(t) = \left(\frac{\mathrm{d}}{\mathrm{d}t} + \lambda\right)^n \int e(t)\mathrm{d}t \tag{24}$$

where n is the system order and λ is a strictly positive constant that helps to define the sliding hyperplane (system bandwidth).

The control objective is to satisfy eq 23; in this case, eq 24 reaches a constant value. To maintain $s(t)$ at this constant value, it is necessary to satisfy

$$\dot{s}(t) = 0 \tag{25}$$

In the traditional sliding-mode control, the control law is the combination of two control actions

$$u = u_c + u_d \tag{26}$$

where u_c is the continuous control action, which is used to maintain the system on the sliding surface, and u_d is the discontinuous control action. It is used to reach the sliding surface.

Developing and deriving eq 24

$$\begin{aligned}\dot{s}(t) &= \mathrm{e}^{(n)}(t) + r_{n-1}\lambda\mathrm{e}^{(n-1)} + r_{n-2}\lambda^2\mathrm{e}^{(n-2)} + \cdots \\ &\quad + r_1\lambda^{(n-1)}\dot{\mathrm{e}}(t) + r_0\lambda^n\mathrm{e}(t) \\ &= \mathrm{e}^{(n)}(t) + \sum_{i=1}^{n} r_{n-i}\lambda^i\mathrm{e}^{(n-i)}\end{aligned} \tag{27}$$

where $\{r_{n-1}, r_{n-2}, \cdots, r_1, r_0\}$ are the terms obtained by solving eq 24 for an exponent n, and $\mathrm{e}^{(0)}(t) = \mathrm{e}(t)$, $r_0 = 1$.

Substituting eq 21 and eq 22 into eq 27, it is obtained

$$\begin{aligned}\dot{s}(t) &= \dot{x}_{dn}(t) - A(X(t), t) - b(X(t), t)u - d(t) \\ &\quad + \sum_{i=1}^{n} r_{n-i}\lambda^i\mathrm{e}^{(n-i)}\end{aligned} \tag{28}$$

For the definition of the continuous control law, $u = u_{nc}$ in eq 28

$$\begin{aligned}\dot{s}(t) &= \dot{x}_{dn}(t) - A(X(t), t) - b(X(t), t)u_{nc} - d(t) \\ &\quad + \sum_{i=1}^{n} r_{n-i}\lambda^i\mathrm{e}^{(n-i)}\end{aligned} \tag{29}$$

Furthermore, the control action is defined as

$$\begin{aligned}u_{nc} &= \mathrm{LAMDA}_c(\dot{s}) \\ &= \left|\frac{\mathrm{argmax}(\gamma_k)}{\sum_{k=1}^{m}\gamma_k\mathrm{GAD}_{k,\mathrm{argmax}(\dot{s}(t))}}\right| \sum_{k=1}^{m}\gamma_k\mathrm{GAD}_{k,\dot{s}(t)}\end{aligned} \tag{30}$$

where m is the number of classes, GAD is the global adequacy degree computed by LAMDA, and γ_k is a single value specified for each class k.

The objective is to satisfy $\dot{s}(t) = 0$ through an adequate control action u_{nc} in eq 29. The only parameter that is necessary to know is the sign of $b(X(t), t)$ and with this information, establish the rules based on the classes of LAMDA. In this paper, we have selected five classes $m = 5$, defined as NB: negative big, NS: negative small, ZE: zero, PS: positive small, and PB: positive big, values used to establish the rules that allow obtaining the control law u_{nc} required to obtain $\dot{s}(t) = 0$. The classes are standardized between $[-1,1]$,[56,57] with the centers in NB = −1, NS = −0.5, ZE = 0, PS = 0.5, and PB = 1.

If $b(X(t),t) > 0$ in eq 29, it is noted that $\dot{s}(t)$ decreases as u_{nc} increases, and $\dot{s}(t)$ increases as u_{nc} decreases, then the rules that allow obtaining $\dot{s}(t) = 0$ are defined. As an example, if $\dot{s}(t)$ is PB, then significant positive control action u_c is needed to decrease quickly $\dot{s}(t)$. If $\dot{s}(t)$ = ZE (it is the desired condition), then no control action is required, thus u_{nc} = ZE.

Based on this analysis, we propose the table of rules corresponding to the control action of the continuous part, which is shown in Table 2.

Finally, the output u_{nc} is multiplied with a scaling gain $k_c > 0$ to obtain u_c as $u_c = k_c u_{nc}$ to improve the response of the controller.

Now, it is necessary to compute the discontinuous control action u_d that moves the states of the system toward the sliding surface. For this, we select a Lyapunov function of the form

$$V(s(t)) = \frac{1}{2}s(t)^2 \tag{31}$$

The derivative of eq 31 is

$$\dot{V}(s(t)) = s(t)\dot{s}(t) \tag{32}$$

For stability, the derivative of the Lyapunov function must meet the condition

$$s(t)\dot{s}(t) < 0 \tag{33}$$

Replacing eq 29 in eq 33, considering the discontinuous part of the control action $u = u_{nd}$, we have

https://doi.org/10.1021/acsomega.2c05756
ACS Omega 2022, 7, 45301−45313

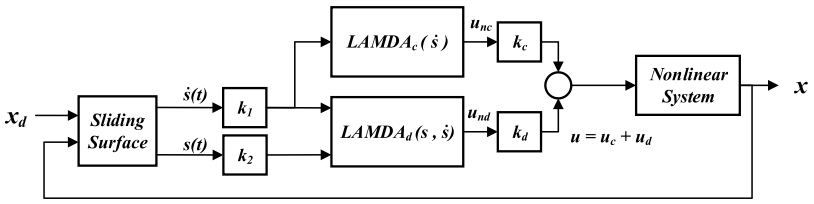

Figure 2. Control scheme of the LSMC.

$$s(t)\dot{s}(t) = s(t)\dot{x}_{dn}(t) - s(t)A(X(t), t) - s(t)b(X(t), t)u_{nd} - s(t)d(t) + s(t)\sum_{i=1}^{n} r_{n-i}\lambda^{i}e^{(n-i)} < 0 \quad (34)$$

And the control action is defined as

$$u_{nd} = \mathrm{LAMDA_d}(s, \dot{s}) = \left|\frac{\mathrm{argmax}(\gamma_k)}{\sum_{k=1}^{m}\gamma_k \mathrm{GAD}_{k,\mathrm{argmax}(\dot{s}(t),s(t))}}\right| \sum_{k=1}^{m}\gamma_k \mathrm{GAD}_{k,(\dot{s}(t),s(t))} \quad (35)$$

As presented in eq 35, u_{nd} is computed for $\dot{s}(t)$ and $s(t)$. In eq 34, if $s(t)\dot{s}(t)$ is negative for all $s(t) \neq 0$, then the sliding mode is guaranteed; that is, the states of the system are attracted from any initial state to the sliding surface.

For the computation of u_{nd}, assuming that $b(X(t), t) > 0$ the table of 25 rules presented in Table 3 is proposed.

As in the case of continuous control action, the output u_{nd} is multiplied with a scaling gain $k_d > 0$ to obtain u_d as $u_d = k_d u_{nd}$ to improve the response of the controller.

The reader must consider that when $b(X(t), t) < 0$ only the signs of the γ_k are changed in Tables 2 and 3. Finally, the control action is

$$u = k_c\mathrm{LAMDA_c}(\dot{s}) + k_d\mathrm{LAMDA_d}(s, \dot{s}) \quad (36)$$

The scaling gains $k_1 > 0$ and $k_2 > 0$ are used to improve the response of the system, considering that the classes are normalized between $[-1, 1]$, and the sliding surface of the different systems do not vary in that range, so they need to be scaled.

The scheme of LSMC is shown in Figure 2, where the blocks of the controller for LAMDA are applied in the continuous and discontinuous parts and the scaling gains in the inputs and the outputs.

3.2. Takagi−Sugeno Sliding-Mode Control (TS−SMC).

A nonlinear system can be represented by Takagi−Sugeno fuzzy systems as shown below

$$\dot{X}(t) = \sum_{i=1}^{n}[A_i X(t) + B_i U(t)]\kappa_i(x_i) \quad (37)$$

where A_i and B_i are constant matrices, obtained around an operating point of the process. $\kappa_i(x_i)$ is known as the firing strength of each fuzzy rule and is calculated as

$$\kappa_i(x_i) = \frac{\omega_i(x_i)}{\sum_{i=1}^{n}\omega_i(x_i)} \quad (38)$$

where $\omega_i(x)$ is a function that depends on the membership degree of x; it is obtained as follows:[58,59]

$$\omega_i(\mu_x) = \prod_{i=1}^{n}\mu_i(x) \quad (39)$$

where $\mu(x_i)$ is the membership degree of x in the different fuzzy regions.

The advantage of using T-S fuzzy systems to represent nonlinear systems is that T-S fuzzy uses linear and readily understandable models and then interpolates them to describe the nonlinear dynamics. Furthermore, using linear models, techniques from linear control, such as gain scheduling, can be used in nonlinear systems[51]

In eq 37, the A_i and B_i matrices are chosen so that the fuzzy system locally represents the system.

With the representation of the system using T-S fuzzy systems, it is possible to design an SMC law that considers the nonlinear dynamics of the process. The design process is similar to the one presented in the section above. The selected sliding surface is the same as in eq 24, but T-S fuzzy systems can adapt the surface to suit better the different operating conditions

$$S(t) = \sum_{i=1}^{n}\left[\left(\frac{\mathrm{d}}{\mathrm{d}t} + \lambda_i\right)^{n}\int e(t)\,\mathrm{d}t\right]\kappa_i(x) \quad (40)$$

Then the control law, using T-S fuzzy systems, can be represented as

$$U(t) = \sum_{i=1}^{n}[u_{c_i} + u_{d_i}]\kappa_i(x) \quad (41)$$

The result is a nonlinear controller with variable gains that change with the operating conditions of the process. A similar approach has been proposed with optimum and PID controllers.[60−62] Since the proposed controller will be used in a process with a long dead time, a Smith predictor structure will be added to the control scheme, as shown in Figure 3.

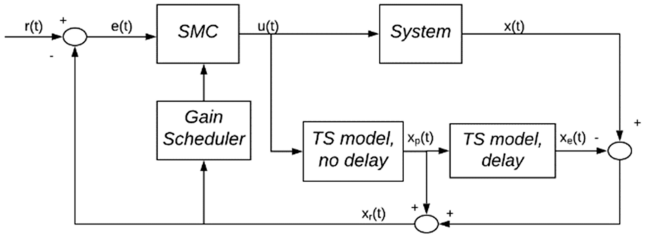

Figure 3. Control scheme for T-S fuzzy SMC.

where:

- T-S model no delay is the fast response using the fuzzy representation of the system.
- T-S model delay is the response taking into account the dead time of the process.
- Gain scheduler adapts the controller parameters.

https://doi.org/10.1021/acsomega.2c05756
ACS Omega 2022, 7, 45301−45313

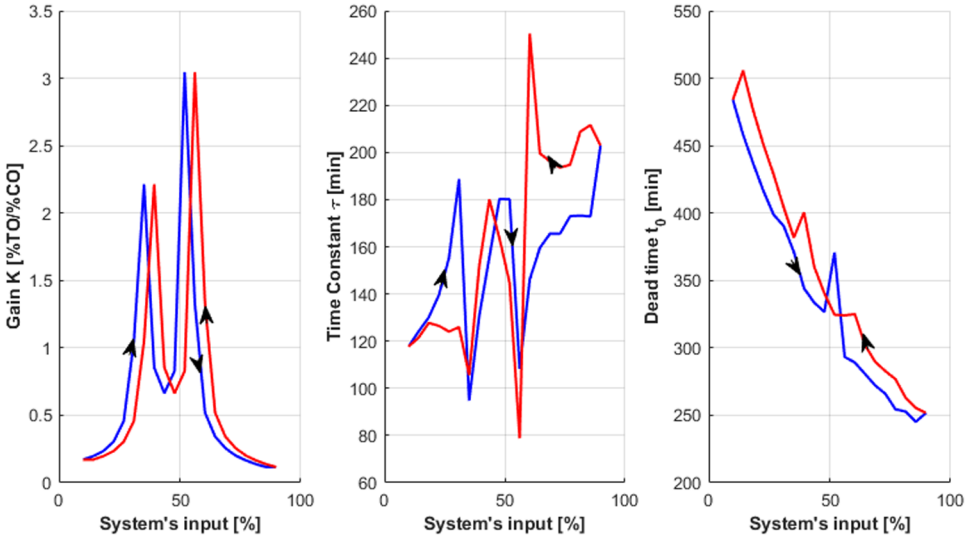

Figure 4. K, τ, and t_0 varying the input of the system.

- SMC is the main controller.
- $r(t)$ is the reference or set point signal.
- $e(t)$ is the error signal.
- $u(t)$ is the control signal.
- $x(t)$ is the process output.
- $x_p(t)$ is the fast estimated output.
- $x_e(t)$ is the estimated output taking into account the system delay.
- $x_r(t)$ is the feedback signal.

4. CONTROLLER DESIGN

4.1. LAMDA Sliding-Mode Control Design. To observe the behavior of the parameters K, τ, and t_0, the procedure presented in ref 51 has been followed, in which it is proposed to vary the input signal [%] applied to the system. Figure 3 shows how these parameters change as a function of the input signal; it goes ascending (blue) and descending (red).

As observed in Figure 4, the parameters change over the entire input signal range, increasing the system's nonlinearity, which is complex to model. Therefore, we consider a nonlinear model due to the time delay, and the variation of the parameters represents an ideal case study to test the LSMC.

The model can be approximated to a first-order plus dead time (FOPDT), as is presented in refs 53 and 68.

$$\frac{X(s)}{U(s)} = \frac{Ke^{-t_0 s}}{\tau s + 1} \tag{42}$$

For the design of the controller, we take as a starting point the modeling of dead time t_0 as proposed,[22] using a first-order Taylor series approximation.

$$e^{-t_0 s} \cong \frac{1}{t_0 s + 1} \tag{43}$$

Substituting eq 43 into eq 42, it is obtained

$$\frac{X(s)}{U(s)} \cong \frac{K}{(\tau s + 1)(t_0 s + 1)} = \frac{K}{\tau t_0 s^2 + (\tau + t_0)s + 1} \tag{44}$$

Solving eq 44 in the time domain

$$\tau t_0 \ddot{x} + (\tau + t_0)\dot{x} + x - Ku = 0 \tag{45}$$

The system is represented in state space, where $x_1 = x$ is

$$\begin{aligned} \dot{x}_1 &= x_2 \\ \dot{x}_2 &= -\frac{(\tau + t_0)}{\tau t_0}x_2 - \frac{1}{\tau t_0}x_1 + \frac{K}{\tau t_0}u \end{aligned} \tag{46}$$

Since this is a second-order differential equation, $n = 2$, the sliding surface $s(t)$ becomes

$$\begin{aligned} s(t) &= \left(\frac{d}{dt} + \lambda\right)^2 \int e(t)dt = \left(\frac{d^2}{dt} + 2\lambda\frac{d}{dt} + \lambda^2\right) \\ &\int e(t)dt = \dot{e}(t) + 2\lambda e(t) + \lambda^2 \int e(t)dt \end{aligned} \tag{47}$$

From eq 47

$$\dot{s}(t) = \ddot{e}(t) + 2\lambda\dot{e}(t) + \lambda^2 e(t) = 0 \tag{48}$$

For $n = 2$ in eq 24

$$\ddot{e}(t) = \dot{x}_{d2}(t) - \dot{x}_2(t) \tag{49}$$

Replacing eq 46 and eq 49 in eq 48

$$\begin{aligned} \dot{s}(t) &= \dot{x}_{d2}(t) + \frac{(\tau + t_0)}{\tau t_0}x_2 + \frac{1}{\tau t_0}x_1 - \frac{K}{\tau t_0}u + 2\lambda\dot{e}(t) \\ &+ \lambda^2 e(t) \\ &= 0 \end{aligned} \tag{50}$$

In Figure 4 it has been shown that $K > 0$ for the entire variation range of the input signal, then $\frac{K}{\tau t_0} > 0$, so, based on the form of eq 28, we can conclude that we have the case $b(X(t), t) > 0$. Thus, the table of rules used in this case study is presented in Tables 2 and 3.

4.2. SMC-TS Controller Design. In practice, the process approach through a FOPDT model is widely used. This is because the FOPDT model captures the dynamic response of the process from which the control system is designed.[63] Furthermore, as proposed in ref 30 a Smith predictor (SP) is ideal for compensating for the time delay. In addition, the SP simplifies the controller's design since it would be enough with a primary control that can be adjusted using delay-free techniques.[64] Thus, since an SP is used and the approximation

https://doi.org/10.1021/acsomega.2c05756
ACS Omega 2022, 7, 45301−45313

Table 4. Parameters for Adaptive SMC-TS[30]

$R(t)$	40	42	44	46	48	50	52	54
λ	0.00924	0.01014	0.01241	0.00786	0.00673	0.00449	0.00247	0.00115
K_d	5.00	4.50	3.80	2.80	3.80	4.70	5.50	5.80
$R(t)$	56	58	60	62	64	66	68	
λ	0.00073	0.00067	0.00077	0.0091	0.00125	0.00201	0.00723	
K_d	3.80	3.50	3.20	2.80	4.50	3.50	2.30	

is accurate, the feedback signal is a first-order system with no dead time.

$$\frac{X_r(s)}{U(s)} = \frac{K}{\tau s + 1} \tag{51}$$

Representing eq 51 in the time domain

$$\dot{x}_r(t) = \frac{K}{\tau}u(t) - \frac{1}{\tau}x_r(t) \tag{52}$$

Given that the system is of the first order, the resulting sliding surface is

$$s(t) = e(t) + \lambda \int e(t)dt \tag{53}$$

Thus

$$\dot{s}(t) = \dot{e}(t) + \lambda e(t) \tag{54}$$

For $n = 1$ in eq 24

$$\dot{e}(t) = \dot{x}_d(t) - \dot{x}_r(t) \tag{55}$$

Replacing eq 52 and eq 55 in eq 54 and solving for $u(t)$ yields the resulting continuous control law

$$u_c(t) = \frac{1}{K}X_r(t) + \frac{\lambda\tau}{K}e(t) \tag{56}$$

The discontinuous control law uses the sigma function to avoid chattering.[22] However, other options, like the super twisting technique, are available to reduce chattering. In refs 65 and 66 are discussed both options considering when it is reasonable to use one of them

$$u_d(t) = K_d\frac{S(t)}{|S(t)| + \delta} \tag{57}$$

The final control law combining eq 56 and eq 57 is

$$u(t) = \frac{1}{K}x_r(t) + \frac{\lambda\tau}{K}e(t) + K_d\frac{S(t)}{|S(t)| + \delta} \tag{58}$$

Using the T-S model to adapt the gains of the controller depending on the operation region, then the sliding surface eq 53 and the control law are now computed as follows

$$S(t) = \sum_{i=1}^{n}\left[e(t) + \lambda_i \int e(t)dt\right]\kappa_i(X) \tag{59}$$

$$u(t) = \sum_{i=1}^{n}\left[\frac{1}{K_i}x_r(t) + \frac{\lambda_i\tau_i}{K_i}e(t) + K_{di}\frac{S_i(t)}{|S_i(t)| + \delta}\right]\kappa_i(X) \tag{60}$$

5. RESULTS AND DISCUSSION

Four approaches are tested to control the process, a conventional PID controller, an SMC controller proposed in ref 67 an SMC-TS,[30] and LSMC. The P.I. controller

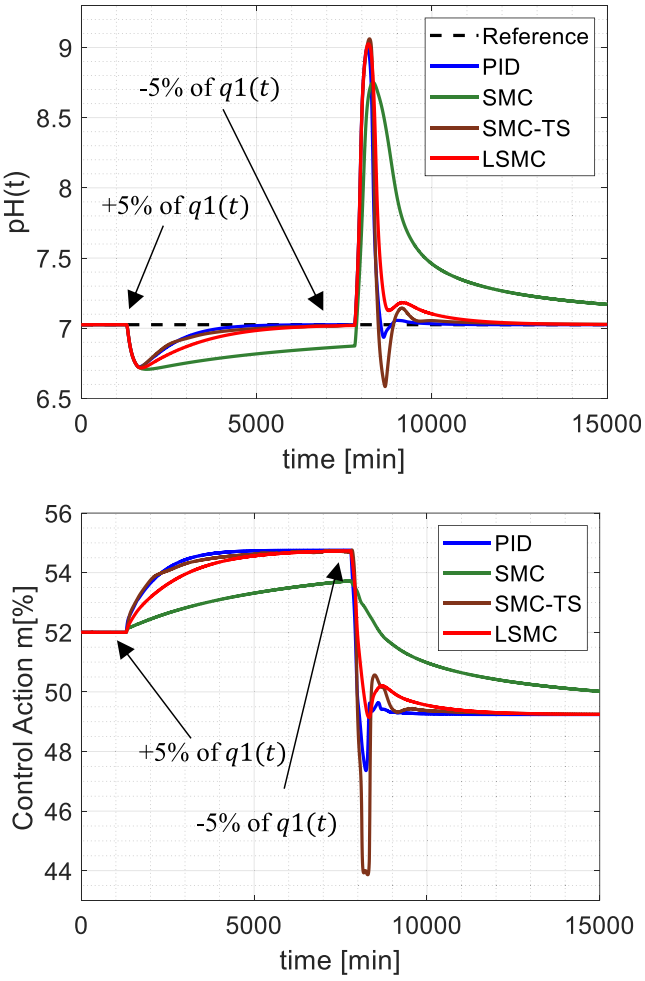

Figure 5. Performance comparison of the controllers when a disturbance in $q1(t)$ affects the system.

Table 5. Performance Metrics of the Controllers When Disturbances Affect the System

controller	ISE	TVU	máximum overshoot %
PID	6.478×10^4	144.2	29.02
SMC	1.585×10^5	120.3	25.01
SMC-TS	7.418×10^4	170.7	29.57
LSMC	8.551×10^4	124.8	29.14

parameters have been tuned considering the method of Dahlin synthesis detailed in ref 68 establishing $K_P = 0.297$, $K_I = 0.033$, and $K_D = 72.79$. The SMC controller parameters have been tuned considering the method proposed in ref 22 these are $\lambda_0 = 0.0000315$, $\lambda_1 = 0.01$, $K_D = 5.35$, and $\delta = 0$, and for the LSMC, empirically we have selected $k_1 = 0.01$, $k_2 = 2$, $k_c = 1$, and $k_d = 32$.

The parameters of SMC-TS are detailed in Table 4 since it is an adaptive controller. The comparison is made with the initial

https://doi.org/10.1021/acsomega.2c05756
ACS Omega 2022, 7, 45301−45313

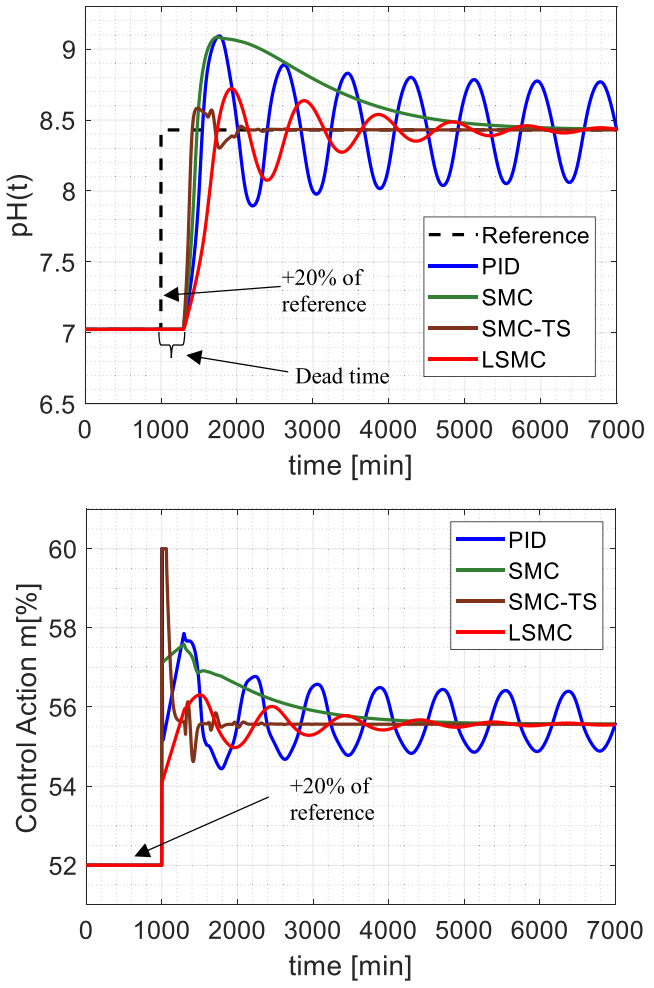

Figure 6. Performance comparison of the controllers in a reference change.

Table 6. Performance Metrics of the Controllers for Reference Changes

controller	ISE	TVU	máximum overshoot %
PID	6.969×10^4	243.6	8.33
SMC	6.501×10^4	123.9	8.10
SMC-TS	3.606×10^4	151.7	2.38
LSMC	5.456×10^4	121.9	4.17

tuned parameters in PID and SMC to analyze their response. First, however, it is necessary to consider that these can be calibrated to improve performance.

The tests carried out in the simulation to validate the controllers have been divided into three parts; these are (a) disturbance rejection to observe how the controllers behave in the face of disturbances applied to the control system, (b) reference changes to see if the controllers are capable of following different desired set point values, (c) reference changes including white noise to the sensor to observe the response of the controllers, and (d) the two case studies combined, that is, multiple reference changes and disturbance rejection.

5.1. Disturbance Rejection. All controller proposals perform well as regulatory controllers for nonlinear processes. For example, Figure 5 shows the response of the controllers when the neutralization process is subjected to a change of

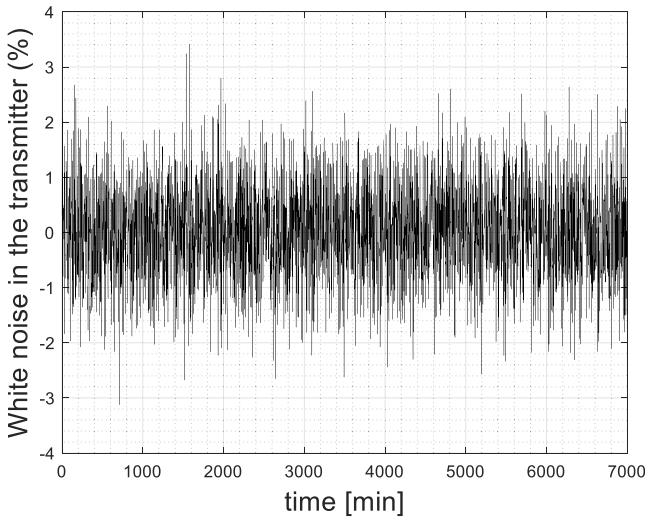

Figure 7. White noise applied to the sensor signal.

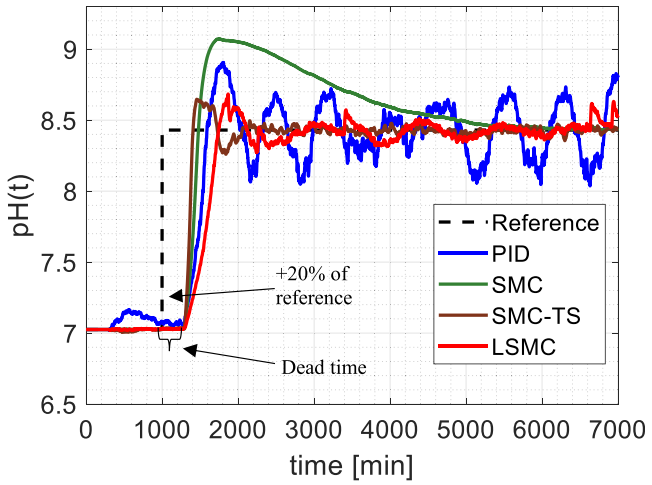

Figure 8. Output of the system considering noise applied to the sensor signal.

+5% in the instant 1000 [min] and of −5% at the time 7500 [min] of $q1(t)$.

Figure 5 shows that the SMC controller presents a reasonably smooth response, requiring more time than the other proposals to reach the reference once the disturbances affect the system. On the other hand, it can be noted that the PID, SMC-TS, and LSMC controllers reach the reference similarly, where the response of the SMC-TS controller stands out, which is more abrupt than PID and LSMC.

Table 5 shows the quantitative analysis of the responses. Three performance metrics have been considered: ISE (integral square error), TVU (control signal effort), and the maximum overshoot obtained by each controller. These results show that the PID and SMC-TS present the best results by minimizing the ISE values but presenting more aggressive control actions, while SMC and LSMC present softer control actions that increase the ISE. In all cases, the values of maximum overshoot are similar.

5.2. Reference Changes. In this simulation, the controllers are tested when the reference changes by 20%. Figure 6 shows that the SMC-TS has the best performance, quickly reaching the set point. The LSMC controller also presents a pretty good response when observing that the

https://doi.org/10.1021/acsomega.2c05756
ACS Omega 2022, 7, 45301−45313

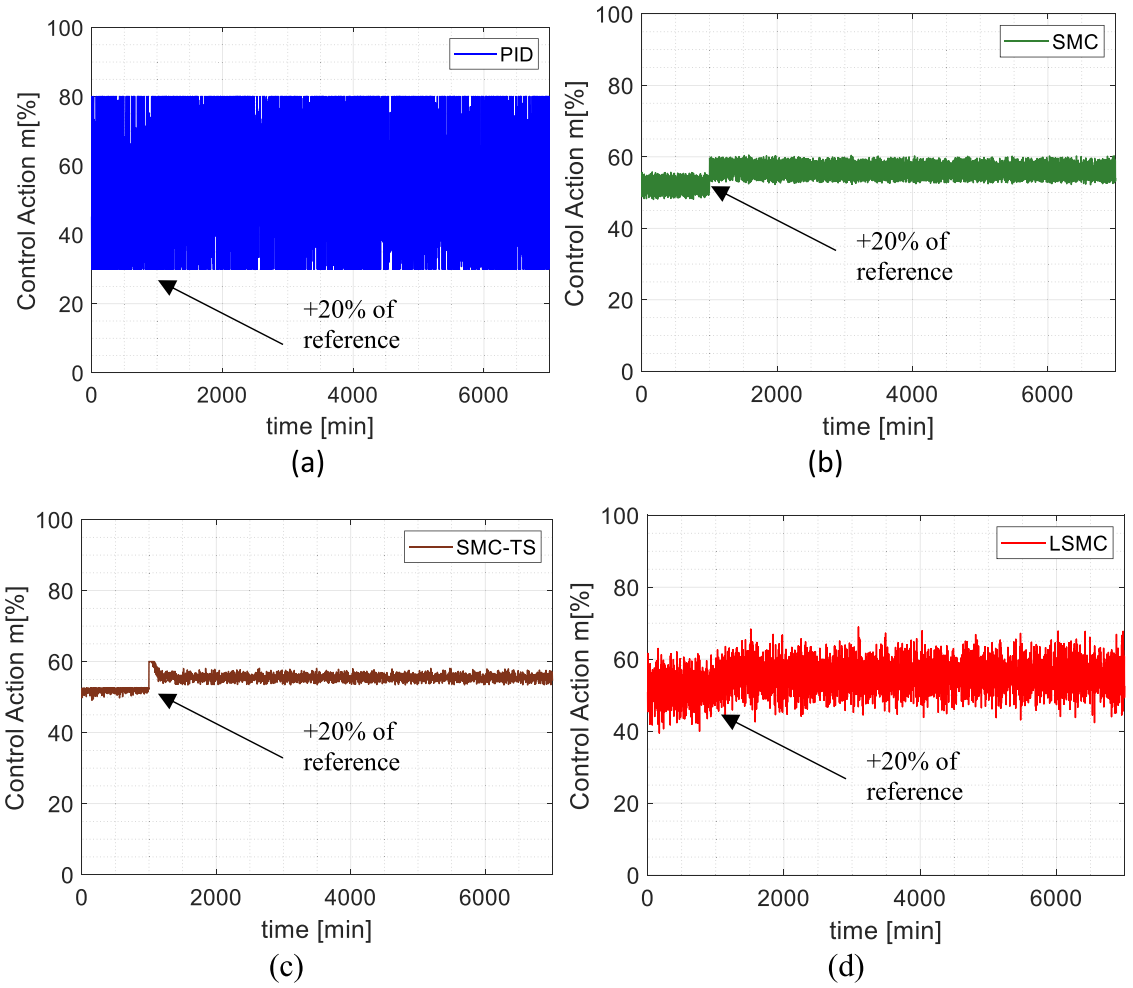

Figure 9. Output of the controllers considering noise applied to the sensor signal (a) PID, (b) SMC, (c) SMC-TS, and (d) LSMC.

Table 7. Performance Metrics of the Controllers for Reference Changes Considering Noise Applied to the Sensor

controller	ISE	TVU
PID	8.009×10^4	5.971×10^4
SMC	7.123×10^4	1.480×10^4
SMC-TS	4.115×10^4	6.422×10^3
LSMC	5.648×10^4	4.050×10^4

reference is reached at 5000 [s]. The SMC controller again gives a slow response when the step signal occurs; however, it gets the reference at a time similar to the LSMC without oscillations. Finally, the controller that degrades its performance is the PID which, due to the parametric calibration of its scaling gains, is more aggressive (which makes it reach the reference quickly, as seen in the previous simulation); in this case, it is oscillatory and does not reach the reference so it can be observed that it decreases its performance.

Table 6 shows quantitatively the performance of the controllers, in which the qualitatively exposed can be seen in Figure 6. In general terms, the LSMC controller is the one that presents a good balance between the ISE, TVU, and maximum overshoot; that is, it presents a response that reaches the reference quickly, with a smooth control action that will not degrade the actuators due to sudden changes of energy.

5.3. Reference Changes Considering Noise in the Sensor Signal. In this simulation, as in the previous section, the controllers have been subjected to a reference change of 20%; however, it has also been considered to add noise to the sensor signal to evaluate the controllers' performance and ability to reach the desired reference. The white noise added to the sensor is presented in Figure 7.

Figure 8 shows the system output obtained by each controller and their respective control actions. Initially, it is observed that the PID is a controller that cannot reach the reference, although it keeps oscillating close to the reference; as seen in Figure 9a, its control action is highly oscillatory, which could affect the actuator considerably. The SMC controller has a slow but noise-immune response that does not change from that shown in Figure 6; its control action shown in Figure 9b is much smoother than that of the PID. The SMC-TS proposal reaches the reference with a fairly fine control action compared to the other proposals (see Figure 9c). Finally, it is observed that the control action of the LSMC (see Figure 9d) is more abrupt than that of the SMC and the SMC-TS; however, it is possible to see that it can reach the desired reference.

Table 7 shows the values of the performance indices of the controllers. The best controller in plant response and control action is SMC-TS, noting that they are considerably less than the other controllers because the control action is the least aggressive, which would be suitable to be applied to the valve.

https://doi.org/10.1021/acsomega.2c05756
ACS Omega 2022, 7, 45301−45313

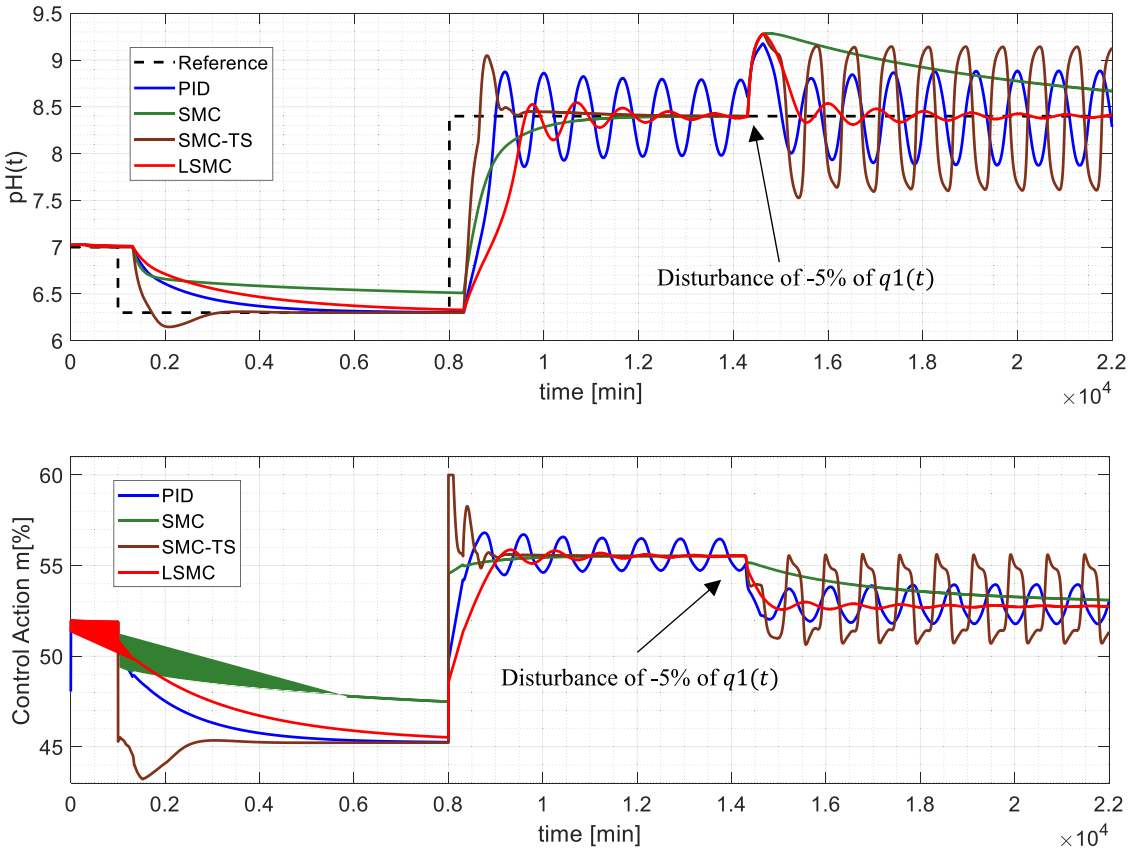

Figure 10. Performance comparison of the controllers for multiple reference changes and disturbance rejection.

Table 8. Performance Metrics of the Controllers for Multiple Reference Changes and Disturbance Rejection

controller	ISE	TVU
PID	2.432×10^5	381.1
SMC	2.690×10^5	156
SMC-TS	2.749×10^5	551.2
LSMC	2.388×10^5	155.9

In terms of ISE, the LSMC controller is the one that follows in performance; however, its control action is more aggressive than that of the SMC as a team, as has been graphically observed.

5.4. Multiple Reference Changes and Disturbance Rejection. Figure 10 shows the response of the controllers when the system is subjected to continuous reference changes of pH(t) in a range between 6.5 and 8.5. With the reference changes, we can see the slow dynamics of the system and how some of the controllers take a long time to reach the reference. Based on the results, SMC-TS is the only controller that reaches each reference; however, when a pH of 8.5 is desired, and a disturbance is applied to the system, the control degrades and presents an oscillatory output that does not reach the reference, being this the weak point of this controller.

In the same way, the PID proposal is oscillatory before the last desired reference. SMC presents a reasonably slow response that is not capable of reaching the reference in any of the cases, and the LSMC proposal is the one that presents the best results, being quite robust before the last reference and being able to recover the system from the disturbance. LSMC is a reasonably balanced proposal for tracking references and rejecting disturbances.

The indices are shown in Table 8, and these values allow us to verify the behavior of LSMC in these tests, showing that the ISE performance index decreases with a low TVU. Based on the measured indices, we can determine that LSMC is the better approach for robustness and disturbance rejection because it preserves stability achieving the desired reference.

6. CONCLUSIONS

This work proposed two hybrid control topologies: artificial intelligence and sliding-mode control theories. The first controller included a LAMDA approach with sliding-mode control, and the second one a Takagi−Sugeno multimodel approach with sliding-mode control. A nonlinear pH neutralization process was used to simulate both approaches. The implementation was analyzed and verified by simulation, and performance indices were used to compare the proposed two approaches quantitatively. The results indicate that these control schemes improve the performance and robustness of the pH process under study.

We can observe by including an artificial intelligence approach, LAMDA or Takagi−Sugeno, with sliding-mode control: (1) During disturbance rejection, the LSMC and SMC-TS controllers present a faster response than SMC and as fast response as PID. Although their maximum overshoots are similar to those of PID, they are more sudden than SMC responses. (2) While SMC-TS has the best performance during reference changes because quickly reaching the set point, LSMC controller response joins the reference with some oscillations but with a better time than SMC and lesser oscillations than PID. (3) The SMC-TS reaches each reference during reference changes and rejects disturbances; however,

https://doi.org/10.1021/acsomega.2c05756
ACS Omega 2022, 7, 45301−45313

when a disturbance is applied, the control degrades and presents an oscillatory output that does not reach the reference. On the other hand, the LSMC proposal is the one that presents the best results, being quite robust before the last reference and being able to recover the system from the disturbance. Therefore, LSMC is a reasonably balanced proposal for tracking references and rejecting disturbances.

Finally, sliding-mode control can overcome the system's uncertainty and robustness to the disturbance and unmodeled dynamics; it has a good control effect on the nonlinear system when changes in the operating conditions of the process occur.

AUTHOR INFORMATION

Corresponding Author

Oscar Camacho − *Colegio de Ciencias e Ingenierías "El Politécnico", Universidad San Francisco de Quito USFQ, Quito 170157, Ecuador;* orcid.org/0000-0001-8827-5938; Email: ocamacho@usfq.edu.ec

Authors

Luis Morales − *Departamento de Automatización y Control Industrial, Escuela Politénica Nacional, Quito 170517, Ecuador*

Juan Sebastian Estrada − *Department of Electronics Engineering, Universidad Técnica Federico Santa María, Valparaıso 2340000, Chile*

Marco Herrera − *Departamento de Automatización y Control Industrial, Escuela Politénica Nacional, Quito 170517, Ecuador*

Andres Rosales − *Departamento de Automatización y Control Industrial, Escuela Politénica Nacional, Quito 170517, Ecuador*

Paulo Leica − *Departamento de Automatización y Control Industrial, Escuela Politénica Nacional, Quito 170517, Ecuador*

Silvana Gamboa − *Departamento de Automatización y Control Industrial, Escuela Politénica Nacional, Quito 170517, Ecuador*

Complete contact information is available at: https://pubs.acs.org/10.1021/acsomega.2c05756

Author Contributions

O.C. conception of the idea, preparation of the first draft, and review of the final manuscript. L.M. and S.E. made simulations and graphs besides designing the initial draft and reviewed the final manuscript. M.H, A.R., P.L., and S.G. reviewed and helped with the final manuscript.

Notes

The authors declare no competing financial interest.

ACKNOWLEDGMENTS

Oscar Camacho thanks the Universidad San Francisco de Quito for supporting this work through the Poli-Grants Program under Grant 17461.

REFERENCES

(1) Wright, R. A.; Kravaris, C. Nonlinear Control of pH Processes Using the Strong Acid Equivalent. *Ind. Eng. Chem. Res.* **1991**, *30*, 1561−1572.

(2) Faanes, A.; Skogestad, S. pH-neutralization: Integrated process and control design. *Comput. Chem. Eng.* **2004**, *28*, 1475−1487.

(3) Singh, P.; Bhanot, S.; Mohanta, H. Neural Control of Neutralization Process using Fuzzy Inference System based Lookup Table. *Int. J. Comput. Appl.* **2013**, *61*, 16−22.

(4) Kambale, S. D.; George, S.; Zope, R. G. Controllers used in pH Neutralization Process: A Review. *Int. Res. J. Eng. Technol.* **2015**, *2*, 354−361.

(5) Ali, E. pH control using P.I. control algorithms with automatic tuning method. *Chem. Eng. Res. Des.* **2001**, *79*, 611−620.

(6) Shahraz, A.; Boozarjomehry, R. B. A fuzzy sliding mode control approach for nonlinear chemical processes. *Control Eng. Pract.* **2009**, *17*, 541−550.

(7) Ram, S.; Kumar, D. D.; Meenakshipriya, B. Designing of PID Controllers for pH Neutralization Process. *Indian J. Sci. Technol.* **2016**, *9*, 1−5.

(8) Chen, J.; Chao, D.; Guo, Q. In *Sliding Mode Control Based on LTR Observer for pH Neutralization Process*, IEEE 6th Data-Driven Control Learning Systems (DDCLS); IEEE: Chongqing, China, 2017; pp 721−726.

(9) Estofanero, L.; Edwin, R.; Garcia, C. Predictive controller applied to a pH neutralization process. *IFAC-PapersOnLine* **2019**, *52*, 202−206.

(10) Herrera, M.; Camacho, O.; Leiva, H.; Smith, C. An approach of dynamic sliding mode control for chemical processes. *J. Process Control* **2020**, *85*, 112−120.

(11) Proano, P.; Capito, L.; Rosales, A.; Camacho, O. In *A Dynamical Sliding Mode Control Approach for Long Dead-Time Systems*, 4th International Conference on Control, Decision and Information Technologies (CoDIT); IEEE: Barcelona, Spain, 2017; pp 0108−0113.

(12) Sira-Ramirez, H. Dynamical sliding mode control strategies in the regulation of nonlinear chemical processes. *Int. J. Control* **1992**, *56*, 1−21.

(13) Slotine, J. J. E.*Applied Nonlinear Control*; Prentice-Hall: Englewood Cliffs, 2014.

(14) Utkin, V.; Poznyak, A.; Orlov, Y. V.; Polyakov, A.*Road Map for Sliding Mode Control Design*; Springer Nature, 2020.

(15) Dhanasekar, R.; Kumar, S. G.; Rivera, M. In *Sliding Mode Control of Electric Drives/Review*, IEEE International Conference on Automatica (ICA-ACCA); IEEE: Curico, Chile, 2016; pp 1−7.

(16) Dominguez, X.; Camacho, O.; Leica, P.; Rosales, A. In *A Fixed-Frequency Sliding-Mode Control in a Cascade Scheme for the Half-Bridge Bidirectional DC-DC Converter*, IEEE Ecuador Technical Chapters Meeting (ETCM) 2016; IEEE: Guayaquil, Ecuador, 2016.

(17) Capito, L.; Proaño, P.; Camacho, O.; Rosales, A.; Scaglia, G. Experimental comparison of control strategies for trajectory tracking for mobile robots. *Int. J. Autom. Control* **2016**, *10*, No. 308.

(18) Mera, M.; Ríos, H.; Martínez, E. A. A sliding-mode based controller for trajectory tracking of perturbed Unicycle Mobile Robots. *Control Eng. Pract.* **2020**, *102*, No. 104548.

(19) Salinas, L. R.; Santiago, D.; Slawiński, E.; Mut, V. A.; Chavez, D.; Leica, P.; Camacho, O. P+d Plus Sliding Mode Control for Bilateral Teleoperation of a Mobile Robot. *Int. J. Control. Autom. Syst.* **2018**, *16*, 1927−1937.

(20) Yang, H.; Liu, L.; Wang, Y. Observer-based sliding mode control for bilateral teleoperation with time-varying delays. *Control Eng. Pract.* **2019**, *91*, No. 104097.

(21) Camacho, O. A Predictive Approach based-Sliding Mode Control. *IFAC Proc. Vol.* **2002**, *35*, 381−385.

(22) Camacho, O.; Smith, C. A. Sliding mode control: An approach to regulate nonlinear chemical processes. *ISA Trans.* **2000**, *39*, 205−218.

(23) Rojas, R.; Camacho, O.; González, L. A sliding mode control proposal for open-loop unstable processes. *ISA Trans.* **2004**, *43*, 243−255.

(24) Rasul, T.; Pathak, M. In *Control of Nonlinear Chemical Process Using Sliding Mode Control*, IEEE International Conference on Power Electronics. Intelligent Control and Energy Systems (ICPEICES-2016); IEEE: Delhi, India, 2016; pp 1−5.

(25) Mehta, U.; Kaya, I. Smith predictor with sliding mode control for processes with large dead times. *J. Electr. Eng.* **2017**, *68*, 463−469.
(26) Mihoub, M.; Nouri, A. S.; Abdennour, R. B. Real-time application of discrete second-order sliding mode control to a chemical reactor. *Control Eng. Pract.* **2009**, *17*, 1089−1095.
(27) Musmade, B. B.; Munje, R.; Patre, B. M. Design of Sliding Mode Controller to Chemical Processes for Improved Performance. *Int. J. Control Autom.* **2011**, *4*, 15−31.
(28) Wang, H.; Wang, Z.; Zhou, Q.; Liang, J.; Yin, Y.; Su, W.; Wang, G. Optimization and Sliding Mode Control of Dividing-Wall Column. *Ind. Eng. Chem. Res.* **2020**, *59*, 20102−20111.
(29) Cargua-Sagbay, D.; Palomo-Lema, E.; Camacho, O.; Alvarez, H. Flash Distillation Control Using a Feasible Operating Region: A Sliding Mode Control Approach. *Ind. Eng. Chem. Res.* **2020**, *59*, 2013−2024.
(30) Estrada, J. S.; Camacho, O. In *Adaptive Sliding Mode Control for a pH Neutralization Reactor: An approach based on Takagi-Sugeno Fuzzy Multimodel*, IEEE Fifth Ecuador Technical Chapters Meeting (ETCM); IEEE: Cuenca, Ecuador, 2021; pp 1−6.
(31) Galan, O.; Romagnoli, J. A.; Palazoglu, A. Real-time implementation of multilinear model-based control strategies−−an application to a bench-scale pH neutralization reactor. *J. Process Control* **2004**, *14*, 571−579.
(32) Cho, J.; Principe, J. C.; Erdogmus, D.; Motter, M. A. Quasi-sliding mode control strategy based on multiple-linear models. *Neurocomputing* **2007**, *70*, 960−974.
(33) Böling, J. M.; Seborg, D. E.; Hespanha, J. P. Multi-model adaptive control of a simulated pH neutralization process. *Control Eng. Pract.* **2007**, 663−672.
(34) Arslan, E.; Çamurdan, M. C.; Palazoglu, A.; Arkun, Y. Multimodel scheduling control of nonlinear systems using gap metric. *Ind. Eng. Chem. Res.* **2004**, *43*, 8275−8283.
(35) Park, B.; Kim, J. W.; Lee, J. M. Data-driven offset-free multilinear model predictive control using constrained differential dynamic programming. *J. Process Control* **2021**, *107*, 1−16.
(36) Ahmadi, M.; Rikhtehgar, P.; Haeri, M. A multimodel control of nonlinear systems: A cascade decoupled design procedure based on stability and performance. *Trans. Inst. Meas. Control* **2020**, *42*, 1271−1280.
(37) Zhu, H.; Shen, J.; Lee, K. Y.; Sun, L. Multi-model based predictive sliding mode control for bed temperature regulation in circulating fluidized bed boiler. *Control Eng. Pract.* **2020**, *101*, No. 104484.
(38) Wang, P.; Chen, Z.; Liao, L.; Wan, J.; Wu, S. A multiple-model based internal model control method for power control of small pressurized water reactors. *Energy* **2020**, *210*, No. 118527.
(39) Tan, W.; Marquez, H. J.; Chen, T.; Liu, J. Multimodel analysis and controller design for nonlinear processes. *Comput. Chem. Eng.* **2004**, *28*, 2667−2675.
(40) Prasad, G. M.; Rao, A. S. Evaluation of gap-metric based multimodel control schemes for nonlinear systems: An experimental study. *ISA Trans.* **2019**, *94*, 246−254.
(41) El Ferik, S.; Adeniran, A. A. Modeling and identification of nonlinear systems: A review of the multimodel approach—Part 2. *IEEE Trans. Syst. Man Cybern. Syst.* **2016**, *47*, 1160−1168.
(42) Du, J.; Song, C.; Yao, Y.; Li, P. Multilinear model decomposition of MIMO nonlinear systems and its implication for multilinear model-based control. *J. Process Control* **2013**, *23*, 271−281.
(43) Li, D.; Tao, X.; Li, N.; Li, S. Switched offline multiple model predictive control with polyhedral invariant sets. *Ind. Eng. Chem. Res.* **2017**, *56*, 9629−9637.
(44) Song, C.; Wu, B.; Zhao, J.; Xu, Z. An integrated output space partition and optimal control method of multiple-model for nonlinear systems. *Comput. Chem. Eng.* **2018**, *113*, 32−43.
(45) Morales, L.; Aguilar, J.; Rosales, A.; Pozo-Espin, D. A Fuzzy Sliding-Mode Control Based on Z-Numbers and LAMDA. *IEEE Access.* **2021**, *9*, 117714−117733.
(46) Morales, L.; Aguilar, J.; Camacho, O.; Rosales, A. An intelligent sliding mode controller based on LAMDA for a class of SISO uncertain systems. *Inf. Sci.* **2021**, *567*, 75−99.
(47) Morales, L.; Aguilar, J.; Chávez, D.; Isaza, C. LAMDA-HAD, an Extension to the LAMDA Classifier in the Context of Supervised Learning. *Int. J. Inf. Technol. Decis. Making* **2020**, *19*, 283−316.
(48) Morales, L.; Aguilar, J. An Automatic Merge Technique to Improve the Clustering Quality Performed by LAMDA. *IEEE Access* **2020**, *8*, 162917−162944.
(49) Morales, L.; Lozada, H.; Aguilar, J.; Camargo, E. Applicability of LAMDA as classification model in the oil production. *Artif. Intell. Rev.* **2020**, *53*, 2207−2236.
(50) Andaluz, G. M.; Morales, L.; Leica, P.; Andaluz, V. H.; Palacios-Navarro, G. LAMDA Controller Applied to the Trajectory Tracking of an Aerial Manipulator. *Appl. Sci.* **2021**, *11*, No. 5885.
(51) Morales, L.; Herrera, M.; Camacho, O.; Leica, P.; Aguilar, J. LAMDA Control Approaches Applied to Trajectory Tracking for Mobile Robots. *IEEE Access* **2021**, *9*, 37179−37195.
(52) Henson, M. A.; Seborg, D. E. Adaptive nonlinear control of a pH neutralization process. *IEEE Trans. Control Syst. Technol.* **1994**, *2*, 169−182.
(53) Iglesias, E.Using Fuzzy Logic to Enhance Control Performance of Sliding Mode Control and Dynamic Matrix Control. Ph.D. Dissertation; USF, 2006.
(54) Noroozi, N.; Roopaei, M.; Jahromi, M. Z. Adaptive fuzzy sliding mode control scheme for uncertain systems. *Commun. Nonlinear Sci. Numer. Simul.* **2009**, *14*, 3978−3992.
(55) Roopaei, M.; Jahromi, M. Z. Chattering-free fuzzy sliding mode control in MIMO uncertain systems. *Nonlinear Anal. Theory, Methods Appl.* **2009**, *71*, 4430−4437.
(56) Feng, G. A Survey on Analysis and Design of Model-Based Fuzzy Control Systems. *IEEE Trans. Fuzzy Syst.* **2006**, *14*, 676−697.
(57) Hwang, G.-C.; Lin, S.-C. A stability approach to fuzzy control design for nonlinear systems. *Fuzzy Sets Syst.* **1992**, *48*, 279−287.
(58) Abonyi, J.Fuzzy Model Identification. In *Fuzzy Model Identification for Control*; Birkhäuser: Boston, 2003; pp 87−164.
(59) Johansen, T. A.; Shorten, R.; Murray-Smith, R. On the interpretation and identification of dynamic Takagi-Sugeno fuzzy models. *IEEE Trans. Fuzzy Syst.* **2000**, *8*, 297−313.
(60) Driankov, D.; Palm, R.; Rehfuess, U. In *Takagi-Sugeno Fuzzy Gain-Scheduler*, IEEE International Conference on Fuzzy Systems; IEEE: New Orleans, LA, U.S.A., 1996; pp 1053−1059.
(61) Zhao, Z. Y.; Tomizuka, M.; Isaka, S. Fuzzy Gain Scheduling of PID Controllers. *IEEE Trans. Syst. Man Cybern.* **1993**, *23*, 1392−1398.
(62) Liang, Y.-W.; Xu, S.-D.; Liaw, D.-C.; Chen, C.-C. Cheng-Chang Chen. A study of T-S model-based SMC scheme with application to robot control. *IEEE Trans. Ind. Electron.* **2008**, *55*, 3964−3971.
(63) Muresan, C. I.; Ionescu, C. M. Generalization of the FOPDT model for identification and control purposes. *Processes* **2020**, *8*, No. 682.
(64) Sanz, R.; García, P.; Albertos, P. A generalized smith predictor for unstable time-delay SISO systems. *ISA Trans.* **2018**, *72*, 197−204.
(65) Pérez-Ventura, U.; Leonid, F. When is it reasonable to implement the discontinuous sliding-mode controllers instead of the continuous ones? Frequency domain criteria. *Int. J. Robust Nonlinear Control* **2019**, *29*, 810−828.
(66) Abdalla, S.; Utkin, V. In *Chattering Analysis of Conventional and Super Twisting Sliding Mode Control Algorithm*, 14th International Workshop on Variable Structure Systems (VSS); IEEE: Nanjing, China, 2016.
(67) Iglesias, E.; García, Y.; Sanjuan, M.; Camacho, O.; Smith, C. Fuzzy surface-based sliding mode control. *ISA Trans.* **2007**, *46*, 73−83.
(68) Smith, C.; Corripio, A.*Principles and Practice of Automatic Process Control*, 3rd ed.; John Wiley & Sons, Inc., 2006.

https://doi.org/10.1021/acsomega.2c05756
ACS Omega 2022, 7, 45301−45313